Biochemistry and Biophysics Reports 2 (2015) 14–22

Contents lists available at ScienceDirect

Biochemistry and Biophysics Reports

journal homepage: www.elsevier.com/locate/bbrep

A novel binding of GTP stabilizes the structure and modulates the activities of human phosphoglucose isomerase/autocrine motility factor

Hua-Yang Lin [a], Jyung-Hurng Liu [b,c,d], Ka-Lik Cheng [a], Jia-Yun Lin [a], Ni-Rung Liu [a], Menghsiao Meng [a,*]

[a] Graduate Institute of Biotechnology, National Chung Hsing University (NCHU), 250 Kuo-Kuang Road, Taichung, Taiwan 40227
[b] Graduate Institute of Genomics and Bioinformatics, NCHU, Taichung, Taiwan 40227
[c] Agricultural Biotechnology Center (ABC), NCHU, Taichung, Taiwan 40227
[d] Rong Hsing Research Center for Translational Medicine, NCHU, Taichung, Taiwan 40227

ARTICLE INFO

Article history:
Received 26 February 2015
Received in revised form
13 April 2015
Accepted 13 April 2015
Available online 30 April 2015

Keywords:
Phosphoglucose isomerase
Glucose-6-phosphate isomerase
Autocrine motility factor
GTP
Inhibition kinetics

ABSTRACT

Phosphoglucose isomerase (PGI) catalyzes the interconversion between glucose 6-phosphate and fructose 6-phosphate in the glycolysis pathway. In mammals, the enzyme is also identical to the extracellular proteins neuroleukin, tumor-secreted autocrine motility factor (AMF) and differentiation and maturation mediator for myeloid leukemia. Hereditary deficiency of the enzyme causes non-spherocytic hemolytic anemia in human. In the present study, a novel interaction between GTP and human PGI was corroborated by UV-induced crosslinking, affinity purification and kinetic study. GTP not only inhibits the isomerization activity but also compromises the AMF function of the enzyme. Kinetic studies, including the Yonetani-Theorell method, suggest that GTP is a competitive inhibitor with a K_i value of 63 μM and the GTP-binding site partially overlaps with the catalytic site. In addition, GTP stabilizes the structure of human PGI against heat- and detergent-induced denaturation. Molecular modelling and dynamic simulation suggest that GTP is bound in a *syn*-conformation with the γ-phosphate group located near the phosphate-binding loop and the ribose moiety positioned away from the active-site residues.

1. Introduction

Phosphoglucose isomerase (PGI, EC 5.3.1.9), ubiquitously present in cytoplasm of most organisms, catalyzes the interconversion between glucose 6-phosphate (G6P) and fructose 6-phosphate (F6P) (Fig. 1) in the glycolysis and gluconeogenesis pathways. In mammal, PGI exhibits diverse functions. It is secreted as neuroleukin by lectin-stimulated T cells to promote the survival of specific embryonic and sensory nerves [1,2]. It is also identical to the autocrine motility factor (AMF) that triggers tumor cell migration [3,4] and a differentiation and maturation mediator that is implicated in the differentiation of myeloid leukemia H-60 cells to terminal monocytic cells [5].

The crystal structures of PGI from a wide range of organisms have been determined [6–11], all folding into a similar architecture. Human PGI (hPGI), for example, is a dimer comprising two identical subunits of ~63 kDa [8]. The individual subunit contains a large and a small domain, each having a parallel β-sheet core surrounded by α-helices. The catalytic site for phosphosugar isomerization is located at a cleft between the large and small domains and is composed of residues from the two neighbouring subunits. A comparison between the native and inhibitor-bound rabbit PGI structures revealed the movement of two loops slightly closer toward the active site upon inhibitor binding [7]. The catalytic site and the region responsible for the AMF function probably overlap because substrate analogues, such as erythrose 4-phosphate and 5-phospho-D-arabinonate, inhibited not only the protein's enzymatic activity but also the AMF function [4,12]. Moreover, a mutation at active-site R273 abolished the enzymatic activity [13] as well as attenuated the cell migration-stimulating function of hPGI [14].

hPGI deficiency shortens the lifespan of red blood cells, causing hereditary non-spherocytic hemolytic anemia (HNSHA). Erythrocytes are a specific cell type due to the absence of nucleus and mitochondrion; therefore, the cells depend on anaerobic conversion of glucose by glycolysis pathway for the generation of NADH and ATP [15]. NADH can be used to reduce methemoglobin to hemoglobin by NADH-cytochrome b5 reductase. ATP provides

* Corresponding author. Tel.: +886 04 22840328; fax: +886 4 22853527.
E-mail address: mhmeng@dragon.nchu.edu.tw (M. Meng).

http://dx.doi.org/10.1016/j.bbrep.2015.04.003

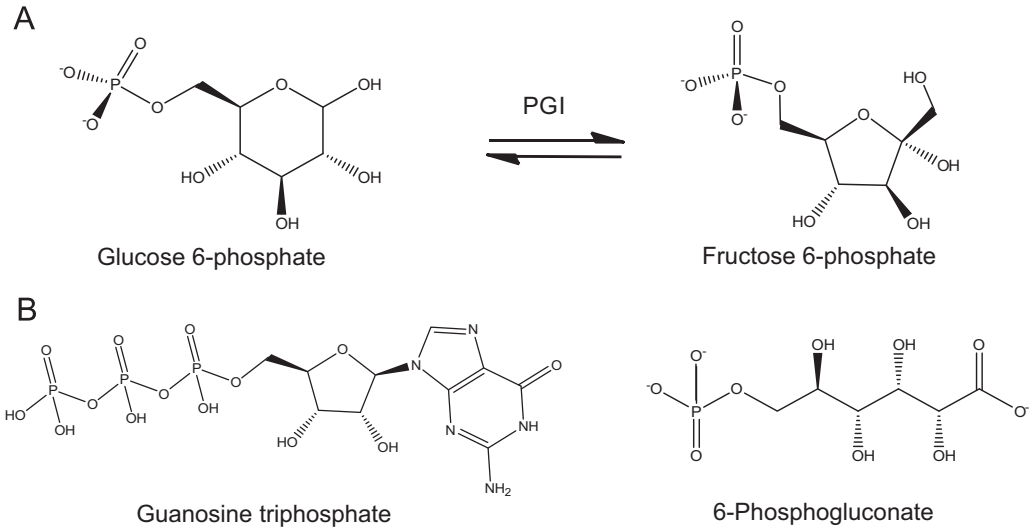

Fig. 1. The isomerization reaction catalyzed by PGI and structures of GTP and 6P-GA.

energy for membrane ion pumps to maintain the electrolyte gradient between plasma and red cell cytoplasm. ATP is also needed for glutathione synthesis and plays a crucial role in nucleotide metabolism. Approximately thirty genetic mutations associated with this genetic disorder have been identified [16,17]; they cause either unstable proteins or proteins impaired in isomerization activity [13,18]. Without the continuous supply of PGI, due to the absence of nucleus, the red blood cells carrying the deficient versions of hPGI would have shorter lifespans, leading to haemolytic anemia.

ATP participates in the activity regulation of a couple of key enzymes in sugar metabolic pathways. It exerts an allosteric inhibition on the activity of phosphofructokinase [19] and pyruvate kinase [20], thus reducing the flux of glycolysis when the cellular ATP concentration becomes ample. The activity of glucose 6-phosphate dehydrogenase (G6PDH) in the pentose phosphate pathway is also inhibited by ATP [21,22] and, to a lesser extent, CTP and GTP [22]. In this study, GTP was found, for the first time, to bind to hPGI. Effects of the GTP binding on the structural stability and catalytic function of hPGI were investigated. The possible GTP-binding mode on hPGI was modelled with the docking software and molecular dynamic simulation.

2. Materials and methods

2.1. Protein preparation

The cDNA of hPGI was obtained by PCR from a human liver cDNA library (Stratagene) as described previously [13]. The cDNA was inserted into plasmid pETDuet (Novagen), and the recombinant plasmid was transformed into *E. coli* BL21(DE3). To express the N-terminally His-tagged hPGI, IPTG (final 10 μM) was added into a 500 ml LB culture when the OD_{600} reached ~1.0; the incubation was continued at 18 °C for 16 h. After recovery by centrifugation, the cell pellet was suspended in 20 ml lysis buffer (40 mM TRICINE, pH 7.5) and homogenized by sonication at 4 °C. The clarified supernatant was loaded onto a 5 ml Ni^{2+}-NTA column, followed by wash and elution with 20 mM and 500 mM imidazole-containing lysis buffer, respectively. The collected protein solution was passed through a DEAE-Sepharose column (12 × 2.5 cm), and the flow-through was loaded onto a Sephacryl S-300 gel filtration column (60 × 1.6 cm) for the further purification of hPGI. The protein concentrations were determined using a Coomassie protein assay kit (Pierce) with bovine serum albumin as the standard.

2.2. Activity assay for isomerization

The enzyme-coupled assay using G6PDH is commonly used to measure the activity of PGI for converting F6P to G6P [13]. However, this method is not applicable to study the inhibition effect of GTP or 6-phosphogluconate (6P-GA) on hPGI, because GTP inhibits G6PDH [22], and so does 6P-GA (data not shown). In this study, the catalytic rate of converting F6P to G6P was determined by an end-point assay. hPGI was first incubated with the indicated amounts of F6P and inhibitors in 1 ml 20 mM HEPES buffer, pH 7.5, at 30 °C for 2–3 min. The reaction was stopped by incubation at 100 °C for 10 min, followed by centrifugation at 13000 × *g*. The amount of G6P produced in the isomerization step was then determined by incubating an aliquot of the reaction solution with 10 units of *Leuconostoc mesenteroids* G6PDH (Sigma-Aldrich) and 2 mM β-NAD^+ in 1 ml HEPES buffer. The increase in the OD_{340} was monitored until it reached a plateau, and the change in the OD_{340} was used to calculate the G6P concentration according to the extinction coefficient of NADH (ε_{340} = 6220 $M^{-1}cm^{-1}$). The amount of hPGI used in the isomerization step was subjected to change to assure that the production of G6P was in the linear range within the incubation period. The apparent kinetic parameters, K_m and V_{max}, were determined according to the dependence of the conversion rate on the F6P concentration using Grafit software (Erithacus Software Ltd., UK). Since both GTP and 6P-GA behaved as competitive inhibitors, their K_i values were calculated based on the plot of the inhibitor concentration versus the apparent K_m. The dependence of the binding sites for GTP and 6P-GA was investigated by the Yonetani – Theorell graphical method [23].

2.3. GTP binding assays

To perform UV-induced crosslinking assay, hPGI (0.7 μg) was mixed with 1 μCi [α-^{32}P]GTP (3000 Ci/mmol/) in an 18 μl solution and placed on ice for 20 min. The reaction mixture was irradiated with UV light (254 nm) for 2 min at a distance of 8 cm using CL1000 ultraviolet crosslinker (UVP, Upland, California). The irradiated product was separated on a 12% SDS-polyacrylamide gel, followed by autoradiography using BAS-2500 Phosphorimager (Fujifilm, Tokyo, Japan).

For GTP-Sepharose binding assay, hPGI (~1 mg) was load onto a 1 ml GTP-Sepharose column (Jena Bioscience, Jena, Germany) that had been equilibrated with 40 mM TRICINE buffer, pH 7.5. After extensive wash with the equilibrium buffer, the protein bound to the column was eluted with the equilibrium buffer that

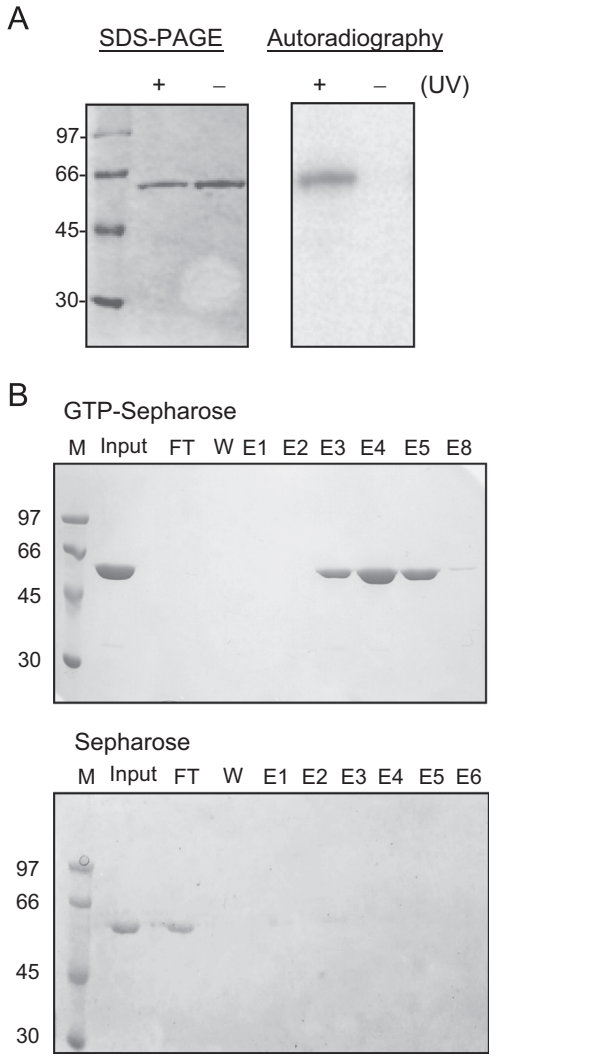

Fig. 2. Binding of GTP to hPGI. (*A*) The UV-induced crosslinking between hPGI and GTP. hPGI was incubated with [α-^{32}P]GTP and then irradiated with UV light at 254 nm as the description under Materials and methods. The irradiated product was subjected to SDS-PAGE, followed by autoradiography. (*B*) Affinity interaction between hPGI and GTP-Sepharose. hPGI was loaded onto a GTP-Sepharose or Sepharose column. After extensive wash, the hPGI bound to the column was eluted by buffer that contained 5 mM GTP. FT, W, and E denote the flow-through, wash, and elution fractions, respectively.

contained 5 mM GTP. The presence of hPGI in every fraction was analysed by SDS-12% PAGE. A parallel experiment using a Sepharose column was conducted as the control.

2.4. Instrumental analyses

To perform circular dichroism (CD) spectropolarimetry, hPGI was adjusted to 40 μg/ml in 2 mM HEPES, pH 7.5, and mixed with the indicated concentration of GTP. The spectrum data, 200–320 nm in 1 nm steps, were obtained using a 0.1-cm pathlength cuvette at 25 °C with a CD spectrometer (J-815, Jasco, Japan).

Differential scanning calorimetry (DSC) was performed using N-DSCIII calorimeter (TA Instruments, New Castle, Delaware). hPGI was dialyzed against 40 mM TRICINE buffer, pH 7.5, and adjusted to a concentration of 0.4 mg/ml with the indicated concentration of GTP, which was prepared in the used dialysis buffer. The protein sample and the used dialysis buffer were loaded into the sample and reference cells, respectively. The scanning temperature started from 20 to 80 °C at the rate of 1 °C/min. Data were analysed with NanoAnalyze Software v2.2.0.

2.5. Blue native polyacrylamide electrophoresis

The stability of the dimeric structure of hPGI against SDS was analyzed by blue native PAGE, which has been used to characterize the oligomeric state of protein complexes [24]. hPGI (10 μg) was mixed with the indicated amounts of SDS and GTP in protein loading buffer, and the protein mixture was incubated at 25 °C for 15 min prior to electrophoresis. The monomer fraction shown on the gel was estimated as pixels with Multi-Gauge software V3.0 (Fujifilm, Tokyo, Japan).

2.6. Cell migration assay

HepG2 hepatoma cells were placed on the top chamber of a transwell cell culture chamber (Corning, New York), fitted with a polycarbonate filter with an 8-μm pore size, at a dose of 2×10^4 cells in 100 μl DMEM supplemented with 10% fetal bovine serum. The bottom chamber was filled with the same medium. After incubation at 37 °C for 24 h, the bottom medium was replaced with the fresh medium that contained 0.16 μM hPGI and/or 100 μM GTP. The cells were allowed to grow for another 16 h. The filter was removed and fixed in 4% paraformaldehyde for 10 min and stained with 0.2% crystal violet for 30 min. The cells on the lower filter surface were counted using an inverted microscope.

2.7. Ligand docking and molecular modelling

The crystal structure of hPGI (PDB ID: 1JLH) [10] was used for the docking experiments. The coordinates of GTP were obtained from PubChem database [25] through the unique chemical structure identifier CID: 6830. The grid box ($30 \times 30 \times 30$Å) was centered at the catalytic site of hPGI. To increase the chance of obtaining the best binding mode, 100 hPGI conformers were randomly built with different side-chain orientations in the catalytic site using MODELLER 9v12 [26]. Each conformer was subjected to GTP docking using AutoDock Vina version 1.1.2 [27]. Each docking run produced 20 binding modes under the exhaustiveness value of 64, and the binding modes were ranked based on their predicted binding affinity (in kcal · mol^{-1}). The top ranked results were visualized and analyzed with PyMOL [28] and its AutoDock plugin [29].

To improve the model quality, the complex model with the best binding affinity score was subjected to molecular dynamics (MD) simulation using GROMACS version 4.6.5 [30] with charmm27 force field. The topology and parameters of GTP compatible with charmm27 force field was generated by SwissParam [31]. The initial structure was immersed in an orthorhombic water box and the net charge was neutralized by the addition of sodium or chloride ions (at 150 mM salt concentration). Long range electrostatics were handled using the particle mesh Ewald method. The steepest descent energy minimization was used to remove possible bad contacts from the initial structures until energy convergence reached 1,000 kJ · mol^{-1} · nm^{-1}. The system was subject to equilibration at 300 K and normal pressure constant (1 bar) for 100 ps under the conditions of position restraints for heavy atoms and LINCS constraints. The equilibrated structure was used to perform the production run with LINCS constraint acting on bonds with hydrogen atoms. The time step of the simulation was set to 2 fs, and the coordinates were saved for analysis every 100 ps.

3. Results

3.1. GTP binds to hPGI

In a UV-induced crosslink experiment aimed to study the GTP-binding activity of a viral mRNA capping enzyme [32], the

Table 1
Effects of a variety of nucleotides on the isomerization activity of hPGI.

Nucleotide	Relative activity (%)[a]
none	100
GTP	52 ± 2
GDP	82 ± 2
GMP	97 ± 4
ATP	91 ± 1

[a] The activity was measured by incubating 10 ng hPGI with 80 μM F6P and 150 μM nucleotide at pH 7.5, 30 °C. The data are the mean of three independent measurements.

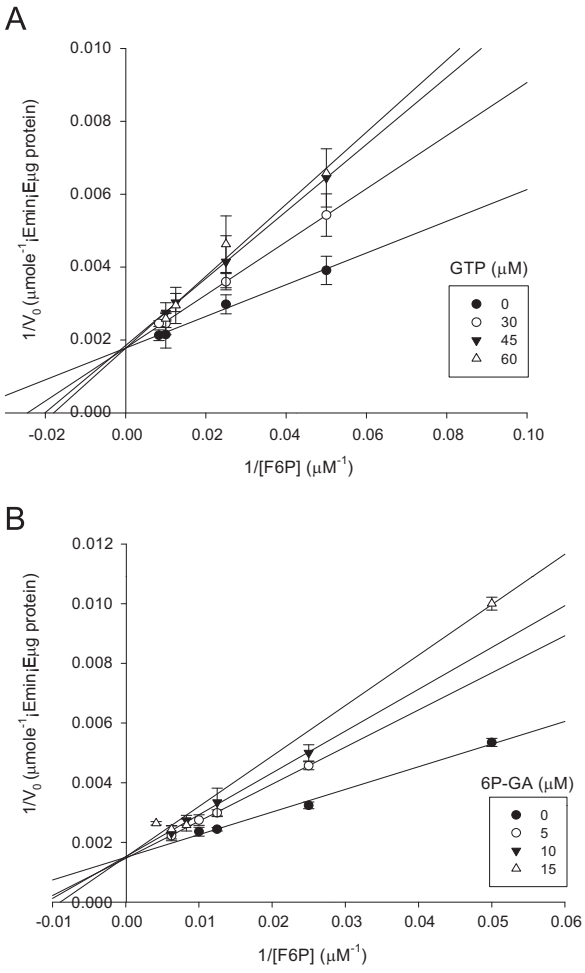

Fig. 3. Competitive inhibition of hPGI by GTP and 6P-GA. The substrate dependence of the initial catalytic rate (v_0) of hPGI in the presence of GTP (0, 30, 45 or 60 μM) (Panel *A*) or 6P-GA (0, 5, 10 or 15 μM) (Panel *B*). Double-reciprocal plots were used to present the data. The reaction condition was as described under Materials and methods. The assay was performed in triplicate.

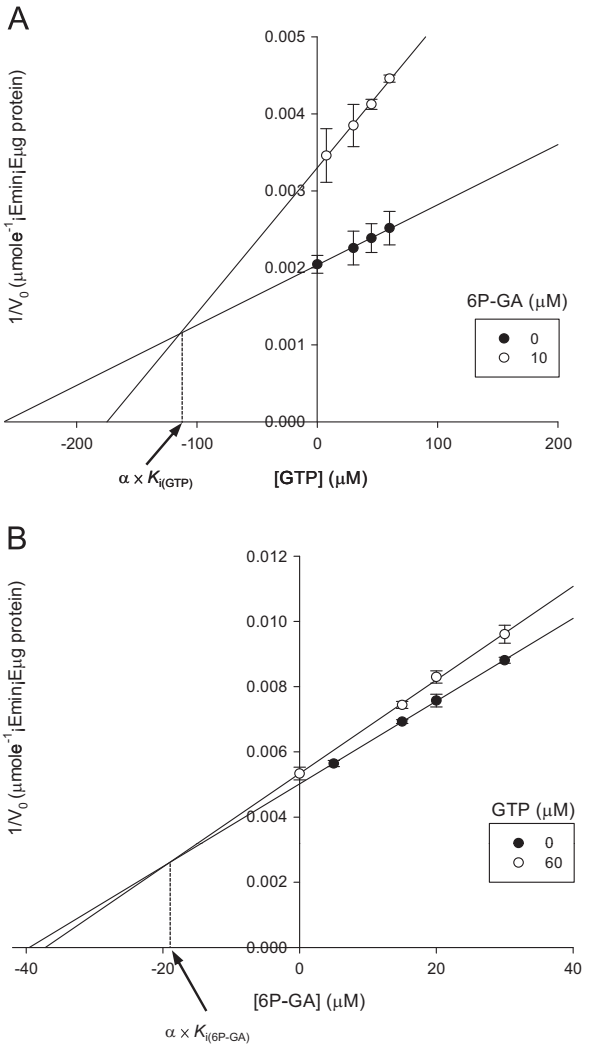

Fig. 4. Yonetani – Theorell plot of the combination of GTP and 6P-GA on hPGI activity. The initial catalytic rate (v_0) of hPGI for F6P (120 μM) isomerization in the simultaneous presence of GTP (0, 7.5, 15, 30, 45 or 60 μM) and 6P-GA (0 or 10 μM) (Panel *A*) or 6P-GA (0, 5, 15, 20 or 30 μM) and GTP (0 or 60 μM) (Panel *B*). The arrow points to the abscissa, from which the α value was calculated. The reaction condition was as described under Materials and methods. The assay was performed in triplicate.

N-terminally His-tag fused hPGI, used as an experimental control, was found linked covalently to [α-^{32}P]GTP after UV irradiation (Fig. 2A). To confirm this unexpected binding activity, the purified hPGI was loaded onto a GTP-Sepharose column, followed by wash and GTP elution (Fig. 2B). The loaded hPGI was fully recovered from the elution fractions, indicating that hPGI could bind to GTP. In a parallel experiment, hPGI passed directly through the Sepharose column. The untagged hPGI, produced in PGI-deficient *E. coli* DF2145 strain and purified using conventional chromatographic columns as described previously [13], was found also able to link covalently to [α-^{32}P]GTP after UV irradiation (data not shown), indicating that the linking between hPGI and GTP was not an artefact due to the presence of the N-terminal His tag.

3.2. GTP competitively inhibits the catalytic activity of hPGI

To determine the significance of the interaction between hPGI and GTP, we first inquired whether hPGI can hydrolyze GTP. hPGI was incubated with [α-^{32}P]GTP in the presence of Mg^{2+}, and the reaction products were analyzed by thin layer chromatography (TLC) using a polyethyleneimine-cellulose plate. GTP hydrolysis, which could be evidenced by the presence of [α-^{32}P]GDP or [α-^{32}P]GMP on the TLC plate, was not detected after incubation up to 4 h (data not shown). Next, we examined whether GTP affects the isomerization activity of hPGI. The activity assay was performed by incubating 10 ng hPGI with 80 μM F6P and 150 μM GTP in 1 ml, pH 7.5 HEPES buffer at 30 °C for 3 min. The G6P produced during this period of time was quantitated by *L. mesenteroids* G6PDH, which catalyzes the oxidation of G6P, accompanied by the reduction of β-NAD^+. Under the reaction condition, GTP decreased the hPGI

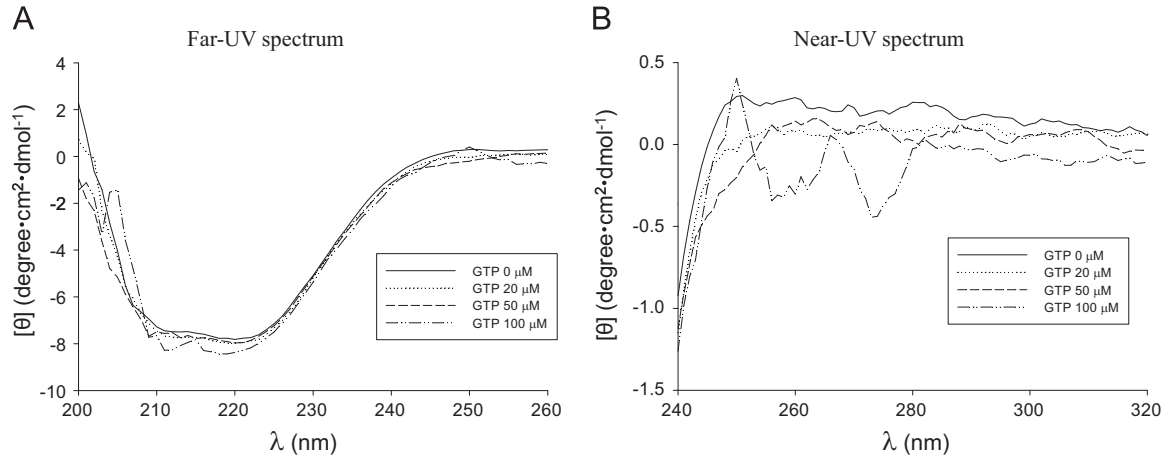

Fig. 5. Effect of GTP on the circular dichroism spectra of hPGI. The far-UV (Panel *A*) and near-UV (Panel *B*) CD spectra of hPGI in the presence of indicated GTP concentrations were measured. The condition was as described under Materials and methods.

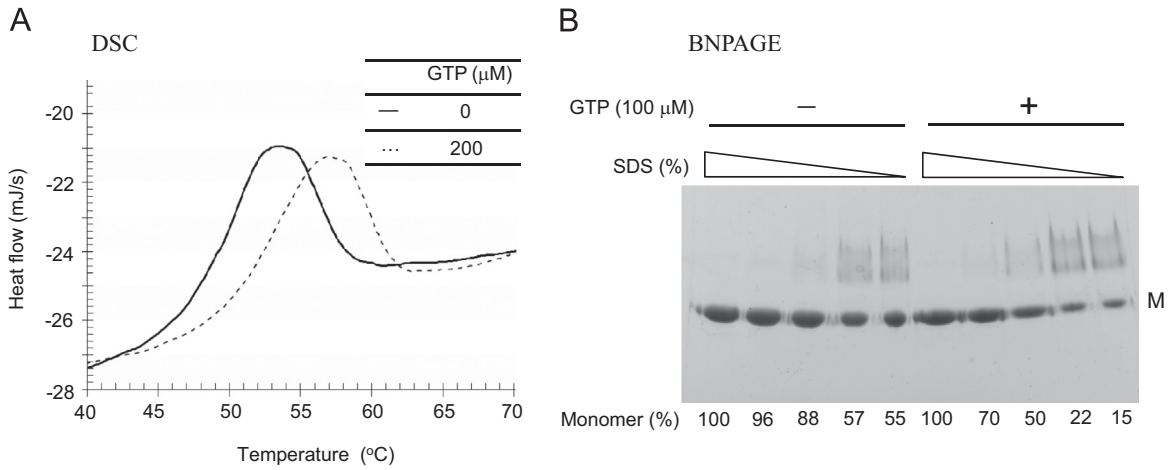

Fig. 6. Effect of GTP on the structural stability of hPGI. (*A*) Differential scanning microcalorimetric (DSC) plots of hPGI were measured in the presence (—) or absence (—) of 200 μM GTP. The measurement condition was as described under Materials and methods. (*B*) hPGI was incubated with SDS (0.01, 0.02, 0.03, 0.05, or 0.1%), in the absence or presence of 100 μM GTP, at 25 °C for 15 min. The samples were then analysed by blue native polyacrylamide gel electrophoresis (BNPAGE) to show the monomer fraction of hGPI.

activity by approximately 50% (Table 1), whereas the inhibitory effects of GDP, GMP, and ATP were minor, indicating that the inhibition caused by GTP was specific.

To elucidate the inhibition mode of GTP, kinetic constants of the hPGI-catalyzed reaction were determined in the absence or presence of GTP (Fig. 3A). In the absence of GTP, K_m and k_{cat} were calculated to be 28 ± 4 μM and 608 ± 36 sec^{-1}, respectively, comparable to those for the untagged hPGI [13]. The presence of GTP, at concentrations of 30, 45, or 60 μM, increased the value of K_m but kept k_{cat} at an approximately constant magnitude. The higher GTP concentration, the greater value of K_m was obtained. These results suggest that GTP is a competitive inhibitor of hPGI. According to the plot of apparent value of K_m versus GTP concentration, the inhibition constant (K_i) of GTP was calculated to be 63 μM. In this study, the inhibitory effect of 6P-GA, presumably a transition state analogue, on the activity of hPGI was also examined (Fig. 3B). As expected, 6P-GA behaved as a stronger competitive inhibitor for hPGI with an apparent K_i of 12 μM.

3.3. The binding sites for GTP and 6P-GA are partially overlapping

Although GTP behaved as a competitive inhibitor, the likelihood of its complete binding to the catalytic site of hPGI was doubted, because GTP structurally differs from F6P and G6P in many ways (Fig. 1). To investigate whether GTP binds to a region overlapping with the catalytic site, the Yonetani–Theorell double-inhibition experiment was carried out by using GTP and 6P-GA as the inhibitors. In the Yonetani–Theorell model, the inhibitor dependence of the velocity (v) follows the eq. (1), in which K_{i1} and K_{i2} are the inhibition constants for inhibitor 1 and 2, respectively [23]. A α value approaching infinity indicates mutually exclusive inhibitor binding, $\infty > \alpha > 1$ suggests a negative effect between the bindings, and $\alpha = 1$ indicates that the two inhibitors bind to the enzyme independently. The reaction velocity of hPGI was first determined at different concentrations of GTP, in the absence or presence of 10 μM 6P-GA simultaneously (Fig. 4A). The plot of the inverse velocity ($1/v$) versus GTP in the absence or presence of 6P-GA led to two intersecting lines (they would be parallel if the value α is infinity). The abscissa of the intersecting point equals the negative value of α times $K_{i(GTP)}$; accordingly, α was calculated to be 1.8. Similarly, the velocity of hPGI was determined at different concentrations of 6P-GA, in the absence or presence of 60 μM GTP simultaneously (Fig. 4B). The plot of $1/v$ versus 6P-GA suggested that α is about 1.6. The α values indicate that GTP and 6P-GA have slightly negative effects on each other's inhibition function, suggesting that the binding sites for GTP and 6P-GA may overlap partly.

$$v = \frac{V_{max}}{1 + \left(\frac{K_m}{A}\right)\left(1 + \frac{I_1}{K_{i1}} + \frac{I_2}{K_{i2}} + \frac{I_1 I_2}{\alpha K_{i1} K_{i2}}\right)} \quad (1)$$

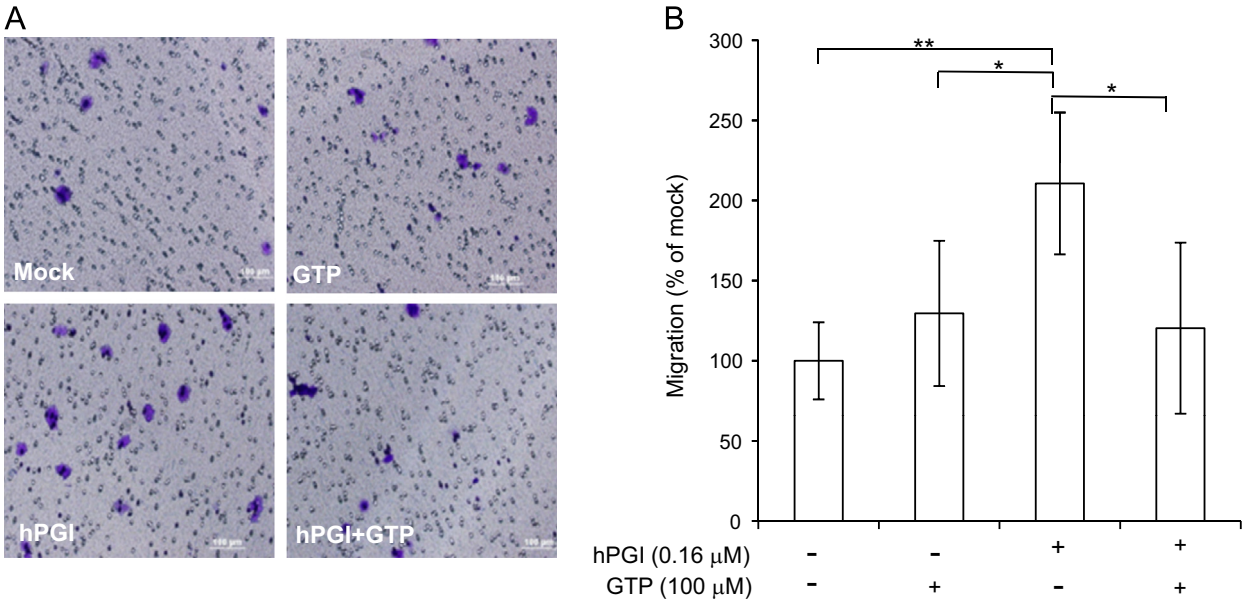

Fig. 7. Suppression of the hPGI-induced cell migration by GTP. (*A*) HepG2 cells migrating across the filter and shown on the lower filter surface. Approximately 2×10^4 cells were placed in the top section of the transwell chamber, and 0.16 μM hPGI and/or 100 μM GTP were added to the lower section. After 16 h of incubation, the cells that migrated across the filter were stained and observed using light microscopy. (Scale bar: 100 μM.) (*B*) Relative migrations of HepG2 cells after the various treatments. Bars show the mean ± S.E.M. of triplicate experiments. $^{*}p < 0.05$, $^{**}p < 0.01$ (T-Test).

3.4. The binding of GTP enhances the structure stability of hPGI

It was of interest to ascertain whether the binding of GTP would affect the conformation of the protein. To answer this question, the influence of GTP on the far- and near-UV CD spectra of hPGI was investigated. The far-UV CD spectrum reflects the secondary structure of the protein, while the near-UV CD spectrum indicates the local conformation around tryptophan and tyrosine. GTP did not affect the far-UV spectrum until its concentration was increased to 100 μM, under which a slight change was observed (Fig. 5A), suggesting that the overall folded structure of hPGI was not significantly affected by the GTP binding. However, the near-UV spectrum changed with the increase of GTP (Fig. 5B). Taken together, a local conformational change might be induced upon the GTP binding. The structural stability of hPGI upon GTP binding was investigated by DSC, a technique that measures the changes of heat capacity during the protein thermal denaturation process, from which the protein melting point (Tm) can be determined. The denaturation of hPGI was monitored from 20 to 80 °C in the absence or presence of 200 μM GTP (Fig. 6A). The presence of GTP increased the Tm from 53 °C to 56.8 °C, indicating that the binding of GTP could stabilize the protein structure against thermal denaturation. Because the isomerization activity of hPGI relies on its dimeric structure, the effect of GTP on the dimer stability was also investigated. The enzyme was incubated with different SDS concentrations (0.01–0.1%) and 100 μM GTP for 15 min, and the mixture was then subjected to blue native PAGE, which had been used to analyze the monomer fraction of hPGI [13]. The monomer fraction shown on the gel increased with the increase of SDS; however, the presence of GTP reduced the degree of monomer dissociation (Fig. 6B).

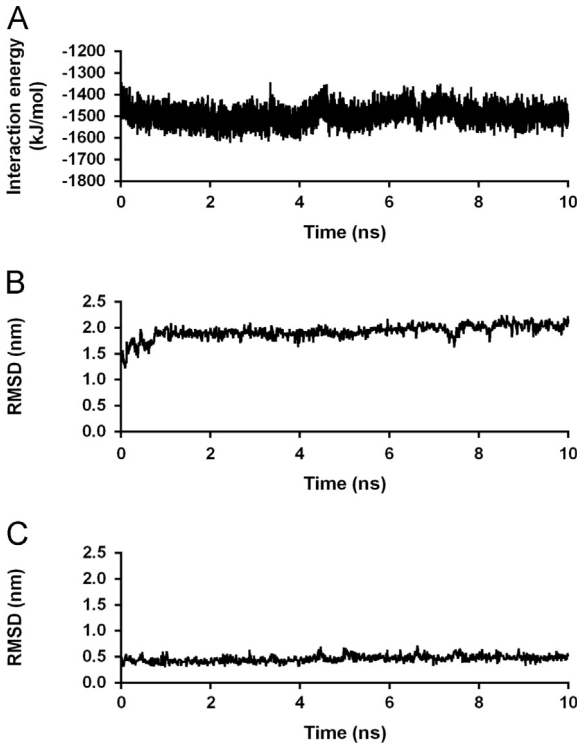

Fig. 8. Analysis of molecular dynamics trajectories generated by GROMACS. Trajectories for (*A*) interaction energy, (*B*) root mean square deviation (RMSD) of residues (Arg96, Gly156, Ile157, Gly158, Gly159, Ser160, Ser210, Lys211, Thr218, Asp268, Gln512, and His389*) in the binding site, (*C*) RMSD of GTP are shown. The interaction energy was estimated as the sum of Coulombic and Lennard-Jones interaction energies between hPGI and GTP.

3.5. GTP interferes with the AMF function of hPGI

The down-regulation of hPGI induced a mesenchymal-to-epithelial transition and suppression of the metastasis of lung fibrosarcoma [33], osteosarcoma [34], and breast cancer cells [35]. Hence, it was important to determine whether GTP affects the AMF function of hPGI. The motility of HepG2 cells was assayed using a transwell cell culture apparatus in response to 0.16 μM hPGI and 100 μM GTP, at which the viability of HepG2 was not

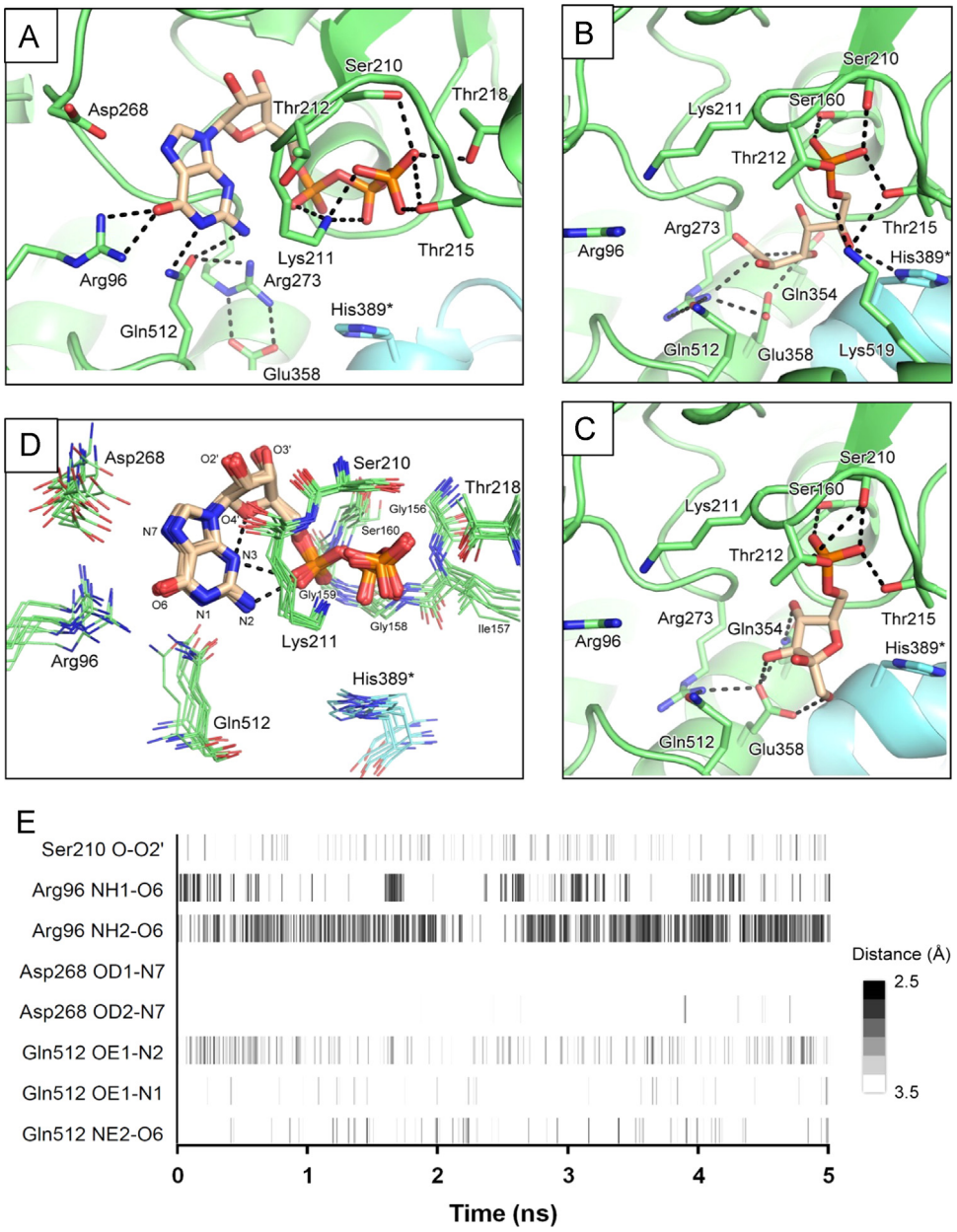

Fig. 9. The predicted binding mode between hPGI and GTP. (*A*) hPGI complexed with GTP modelled in this study. (*B*) The crystal structure of mouse PGI complexed with the inhibitor 6P-GA (PDB ID: 2CXR) [35]. (*C*) The crystal structure of mouse PGI complexed with the substrate F6P (PDB ID: 2CXS) [35]. In panel A-C, subunit A of PGI is colored as green, subunit B as cyan. His389* denotes that the residue His389 comes from subunit B. The ligand is shown as a stick model (ivory, carbon; blue, nitrogen; red, oxygen). Residues involved in ligand binding are shown as stick models. The black dashed lines represent the polar contacts between the ligand and amino acid residues. (*D*) Frames of GTP in the binding site of hPGI during 5 ns of MD simulation. The black dashed lines represent the polar contacts inside the GTP molecule. (*E*) The timeline of hydrogen bonds formed in the binding site during 5 ns of MD simulation. The hydrogen bonds formed between hPGI and GTP are depicted in grayscale lines. The grayscale represents the hydrogen bond distance which gives some indication of the bond strength.

affected. As expected, hPGI at the tested concentration increased the number of cells that migrated across the filter by a factor of approximately 2 (Fig. 7). GTP alone did not significantly affect the motility of HepG2, yet it compromised the migration-stimulating effect of hPGI. This observation, reminiscent of the simultaneous inhibition of the catalytic activity as well as the AMF function of PGI by substrate analogues [4,12], implying that the binding of GTP should involve or alter the substrate-binding pocket. In addition, the ability of GTP to interfere with the AMF function of hPGI raises an interesting question as whether the extracellular GTP concentration is implicated in the metastasis of tumor cells. The relevance between GTP and the malignancy of cancer may deserve a further investigation.

3.6. The docking model of the hPGI-GTP complex

To gain more molecular insight into the inhibitory mechanism of GTP on hPGI activity, the molecular docking study was carried out on the published crystal structure of open form hPGI (PDB ID: 1JLH) [10]. AutoDock Vina [27] docked GTP into the catalytic site with a binding free energy of $-10\ \mathrm{kcal \cdot mol^{-1}}$. Early reports indicated that upon ligand binding, local conformation changes (from open to closed form) occur around the catalytic site [10,36–38]. Therefore, MD simulation was conducted after docking in order to sample the most probable docking poses coupled with the conformational changes. A significant drop in the interaction energy was observed within 1 ns during the simulation,

presumably due to conformation changes in the GTP-binding site (Fig. 8). Because the interaction energy and the conformation of binding site became steady after 5 ns, the simulation was stopped at 10 ns and the trajectory of the final 5 ns was analyzed.

In the binding mode after MD simulation, GTP adopts a *syn*-conformation and the γ-phosphate moiety is located near the phosphate-binding loop (residues 210–216) by virtue of hydrogen-bond interactions to the side chains of Ser210, Thr215 and Thr218 of hPGI (Fig. 9A). In the structure of mouse PGI complexed with 6P-GA (Fig. 9B) or F6P (Fig. 9C), the phosphate group of the ligands also interacts with the phosphate-binding loop by hydrogen-bonding to the side chains of Ser160, Ser210, Thr212 and Thr215 and the main-chain amide groups of Lys211 and Thr212. Nonetheless, a couple of differences are notable in the case of GTP binding; the side chain of Thr212 moves away and is not involved in phosphate binding and that of Lys211 bents down about 60° to interact with the α and β phosphates of GTP (Fig. 9A). The sugar moieties of the bound 6P-GA and F6P are positioned near His389* (comes from the adjacent subunit) [36–38]. Other critical residues involved in the sugar moiety-binding are Arg273, Gln354, Glu358 and Lys519 (Fig. 9B and C). Instead, our docking model shows that the ribose moiety of GTP is located away from His389* and stabilized by a hydrogen bond between its O2' hydroxyl group and the main chain carbonyl group of Ser210 (Fig. 9D).

The residues involved in the recognition of GTP base moiety are Arg96, Asp268 and Gln512 according to the model (Fig. 9A). Based on the 5 ns MD trajectory (Figs. 9D, 9E), the guanidinium group of Arg96 interacts with the O6 carbonyl group of GTP by hydrogen bonds. Gln512 side-chain amide group is able to form hydrogen bonds to N1 amine, N2 amine and/or O6 carbonyl group of GTP. Asp268 is close to the N7 amine group of GTP. However, the role of Asp268 might be minor, because the Asp residue seldom forms a hydrogen bond to an amine group at physiological pH. Thus, it seems likely that Arg96 and Gln512 constitutes the structural basis for the specificity of PGI for GTP. In summary, the triphosphate moiety of GTP may occupy the phosphate-binding pocket of the catalytic site and this would drive a movement of the phosphate-binding loop, leading to a closure of the catalytic site, and thus hindering the entry of substrate.

4. Discussion

The overall velocity of glycolysis has been known to be regulated by three rate-determining enzymes, which are hexokinase, phosphofructokinase, and pyruvate kinase. The activity of hexokinase is subjected to feedback inhibition by G6P and this inhibition is relieved by inorganic phosphate [39]. Phosphofructokinase is allosterically inhibited by ATP, with a K_i value of 0.1 mM at physiological pH [40]. AMP exerts a counteraction to reverse the inhibition. Pyruvate kinase is also regulated by ATP in an allosteric mode. Approximately 30% activity of the enzyme isolated from erythrocytes was inhibited by 0.7-1.3 mM ATP [41]. ATP also regulates the flux of pentose phosphate pathway by competitively inhibiting the activities of G6PDH and 6-phosphogluconate dehydrogenase (6PGD). The K_i value for ATP toward the reaction catalyzed by G6PDH isolated from erythrocyte is about 1.03 ± 0.17 mM [42]. In this study, a specific interaction between hPGI and GTP was identified for the first time. GTP inhibits the activity of hPGI by acting as a competitive inhibitor with a K_i value of 63 μM. In addition, GTP moderately suppresses the AMF function of hPGI. Given the physiological concentration of GTP in mammalian cells being 468 ± 224 μM [43], GTP might be a factor affecting the various biological functions of hPGI by different extents. This proposition deserves being considered in future research regarding this moonlighting protein.

The value of α in the Yonetani-Theorell double-inhibition experiment in this study was approximately 1.7, suggesting that GTP and 6P-GA have a great chance to interfere with each other for the binding to hPGI. The docking model suggests that the binding of the triphosphate moiety of GTP not only triggers the movement of the phosphate-binding loop to the closed form but also induces the bending of Lys211, through which the loop closure is further enforced. GTP binding would therefore block the access of the phosphosugar substrate or 6P-GA to the catalytic site. Nonetheless, this GTP-binding mode remains speculative until the crystal structure of hPGI complexed with GTP is determined.

5. Conclusion

Human phosphoglucose isomerase (hPGI) is a moonlighting protein, performing diverse physiological functions such as catalyzing the isomerization between glucose 6-phosphate and fructose 6-phosphate and promoting the migration of certain cancer cells. This study evidenced a specific binding between GTP and hPGI. To the isomerization activity, GTP acts as a competitive inhibitor. GTP also suppresses the tumor cell migration-stimulating function of hPGI. The Yonetani-Theorell double-inhibition experiment using GTP and 6-phosphogluconate as inhibitors in the isomerization reaction suggested that the GTP-binding site partially overlaps the catalytic pocket of hPGI.

Acknowledgement

This work was supported by grants NSC98-2313-B-005-019-MY3 from the Ministry of Science and Technology, Taiwan, ROC.

Appendix A. Supplementary Information

Supplementary data associated with this article can be found in the online version at http://dx.doi.org/10.1016/j.bbrep.2015.04.003.

References

[1] M. Chaput, V. Claes, D. Portetelle, I. Cludts, A. Cravador, et al., The neurotrophic factor neuroleukin is 90% homologous with phosphohexose isomerase, Nature 332 (1988) 454–455.
[2] P. Faik, J.I. Walker, A.A. Redmill, M.J. Morgan, Mouse glucose-6-phosphate isomerase and neuroleukin have identical 3' sequences, Nature 332 (1988) 455–457.
[3] Y. Niinaka, S. Oida, A. Ishisaki, K. Takeda, T. Iimura, et al., Autocrine motility factor and its receptor expressions in human oral squamous cell carcinoma (SCC) cells, Int J Oncol 9 (1996) 433–438.
[4] H. Watanabe, K. Takehana, M. Date, T. Shinozaki, A. Raz, Tumor cell autocrine motility factor is the neuroleukin/phosphohexose isomerase polypeptide, Cancer Res 56 (1996) 2960–2963.
[5] W. Xu, K. Seiter, E. Feldman, T. Ahmed, J.W. Chiao, The differentiation and maturation mediator for human myeloid leukemia cells shares homology with neuroleukin or phosphoglucose isomerase, Blood 87 (1996) 4502–4506.
[6] C.C. Chou, Y.J. Sun, M. Meng, C.D. Hsiao, The crystal structure of phosphoglucose isomerase/autocrine motility factor/neuroleukin complexed with its carbohydrate phosphate inhibitors suggests its substrate/receptor recognition, J Biol Chem 275 (2000) 23154–23160.
[7] C.J. Jeffery, R. Hardre, L. Salmon, Crystal structure of rabbit phosphoglucose isomerase complexed with 5-phospho-D-arabinonate identifies the role of Glu357 in catalysis, Biochemistry 40 (2001) 1560–1566.
[8] J. Read, J. Pearce, X. Li, H. Muirhead, J. Chirgwin, et al., The crystal structure of human phosphoglucose isomerase at 1.6 A resolution: implications for catalytic mechanism, cytokine activity and haemolytic anaemia, J Mol Biol 309 (2001) 447–463.
[9] C. Davies, H. Muirhead, Crystal structure of phosphoglucose isomerase from pig muscle and its complex with 5-phosphoarabinonate, Proteins 49 (2002) 577–579.
[10] A.T. Cordeiro, P.H. Godoi, C.H. Silva, R.C. Garratt, G. Oliva, et al., Crystal structure of human phosphoglucose isomerase and analysis of the initial catalytic steps, Biochim Biophys Acta 1645 (2003) 117–122.

[11] M. Totir, N. Echols, M. Nanao, C.L. Gee, A. Moskaleva, et al., Macro-to-micro structural proteomics: native source proteins for high-throughput crystallization, PLoS One 7 (2012) e32498.
[12] F.L. Yu, M.H. Liao, J.W. Lee, W.L. Shih, Induction of hepatoma cells migration by phosphoglucose isomerase/autocrine motility factor through the upregulation of matrix metalloproteinase-3, Biochem Biophys Res Commun 314 (2004) 76–82.
[13] H.Y. Lin, Y.H. Kao, S.T. Chen, M. Meng, Effects of inherited mutations on catalytic activity and structural stability of human glucose-6-phosphate isomerase expressed in *Escherichia coli*, Biochim Biophys Acta 1794 (2009) 315–323.
[14] W.L. Shih, M.H. Liao, F.L. Yu, P.Y. Lin, H.Y. Hsu, S.J. Chiu, AMF/PGI transactivates the MMP-3 gene through the activation of Src-RhoA-phosphatidylinositol 3-kinase signaling to induce hepatoma cell migration, Cancer Lett 270 (2008) 202–217.
[15] R. van Wijk, W.W. van Solinge, The energy-less red blood cell is lost: erythrocyte enzyme abnormalities of glycolysis, Blood 106 (2005) 4034–4042.
[16] E. Beutler, C. West, H.A. Britton, J. Harris, L. Forman, Glucosephosphate isomerase (GPI) deficiency mutations associated with hereditary nonspherocytic hemolytic anemia (HNSHA), Blood Cells Mol Dis 23 (1997) 402–409.
[17] W. Kugler, M. Lakomek, Glucose-6-phosphate isomerase deficiency, Baillieres Best Pract Res Clin Haematol 13 (2000) 89–101.
[18] H. Kanno, H. Fujii, S. Miwa, Expression and enzymatic characterization of human glucose phosphate isomerase (GPI) variants accounting for GPI deficiency, Blood Cells Mol Dis 24 (1998) 54–61.
[19] T. Schirmer, P.R. Evans, Structural basis of the allosteric behaviour of phosphofructokinase, Nature 343 (1990) 140–145.
[20] P. del Valle, F. Busto, D. de Arriaga, J. Soler, ATP inhibition of Phycomyces pyruvate kinase: a kinetic study of the inhibitory effects on the allosteric kinetics shown by the enzyme, J Enzyme Inhib 3 (1990) 219–228.
[21] G. Avigad, Inhibition of glucose 6-phosphate dehydrogenase by adenosine 5'-triphosphate, Proc Natl Acad Sci USA 56 (1966) 1543–1547.
[22] P. Ninfali, L. Baronciani, Interaction of ATP with erythroblast glucose-6-phosphate dehydrogenase, Biochem Mol Biol Int 39 (1996) 377–385.
[23] T. Yonetani, The Yonetani-Theorell graphical method for examining overlapping subsites of enzyme active centers, Methods Enzymol 87 (1982) 500–509.
[24] H. Schagger, W.A. Cramer, G. von Jagow, Analysis of molecular masses and oligomeric states of protein complexes by blue native electrophoresis and isolation of membrane protein complexes by two-dimensional native electrophoresis, Anal Biochem 217 (1994) 220–230.
[25] Y. Wang, T. Suzek, J. Zhang, J. Wang, S. He, et al., PubChem BioAssay: 2014 update, Nucleic Acids Res 42 (2014) D1075–1082.
[26] N. Eswar, B. Webb, M.A. Marti-Renom, M.S. Madhusudhan, D. Eramian, et al., Comparative protein structure modeling using MODELLER, Curr Protoc Protein Sci (2007) 9, Chapter 2.
[27] O. Trott, A.J. Olson, AutoDock Vina: improving the speed and accuracy of docking with a new scoring function, efficient optimization, and multithreading, J Comput Chem 31 (2010) 455–461.
[28] W.L. DeLano, The PyMOL Molecular Graphics System. 1.3, Schrödinger, LLC, 2004.
[29] D. Seeliger, B.L. de Groot, Ligand docking and binding site analysis with PyMOL and Autodock/Vina, J Comput Aided Mol Des 24 (2010) 417–422.
[30] S. Pronk, S. Pall, R. Schulz, P. Larsson, P. Bjelkmar, et al., GROMACS 4.5: a high-throughput and highly parallel open source molecular simulation toolkit, Bioinformatics 29 (2013) 845–854.
[31] V. Zoete, M.A. Cuendet, A. Grosdidier, O. Michielin, SwissParam: a fast force field generation tool for small organic molecules, J Comput Chem 32 (2011) 2359–2368.
[32] R.H. Hu, M.C. Lin, Y.H. Hsu, M. Meng, Mutational effects of the consensus aromatic residues in the mRNA capping domain of *Bamboo mosaic virus* on GTP methylation and virus accumulation, Virology 411 (2011) 15–24.
[33] T. Funasaka, H. Hu, T. Yanagawa, V. Hogan, A. Raz, Down-regulation of phosphoglucose isomerase/autocrine motility factor results in mesenchymal-to-epithelial transition of human lung fibrosarcoma cells, Cancer Res 67 (2007) 4236–4243.
[34] Y. Niinaka, K. Harada, M. Fujimuro, M. Oda, A. Haga, et al., Silencing of autocrine motility factor induces mesenchymal-to-epithelial transition and suppression of osteosarcoma pulmonary metastasis, Cancer Res 70 (2010) 9483–9493.
[35] A. Ahmad, A. Aboukameel, D. Kong, Z. Wang, S. Sethi, et al., Phosphoglucose isomerase/autocrine motility factor mediates epithelial-mesenchymal transition regulated by miR-200 in breast cancer cells, Cancer Res 71 (2011) 3400–3409.
[36] J.T. Solomons, E.M. Zimmerly, S. Burns, N. Krishnamurthy, M.K. Swan, et al., The crystal structure of mouse phosphoglucose isomerase at 1.6A resolution and its complex with glucose 6-phosphate reveals the catalytic mechanism of sugar ring opening, J Mol Biol 342 (2004) 847–860.
[37] N. Tanaka, A. Haga, N. Naba, K. Shiraiwa, Y. Kusakabe, et al., Crystal structures of mouse autocrine motility factor in complex with carbohydrate phosphate inhibitors provide insight into structure-activity relationship of the inhibitors, J Mol Biol 356 (2006) 312–324.
[38] N. Tanaka, A. Haga, H. Uemura, H. Akiyama, T. Funasaka, et al., Inhibition mechanism of cytokine activity of human autocrine motility factor examined by crystal structure analyses and site-directed mutagenesis studies, J Mol Biol 318 (2002) 985–997.
[39] J.E. Wilson, Hexokinases, Rev Physiol Biochem Pharmacol 126 (1995) 65–198.
[40] G.E. Staal, J.F. Koster, C.J. Banziger, L. van Milligen-Boersma, Human erythrocyte phosphofructokinase: its purification and some properties, Biochim Biophys Acta 276 (1972) 113–123.
[41] A. Kahn, J. Marie, Pyruvate kinases from human erythrocytes and liver, Methods Enzymol 90 (1982) 131–140.
[42] A. Yoshida, M. Lin, Regulation of glucose-6-phosphate dehydrogenase activity in red blood cells from hemolytic and nonhemolytic variant subjects, Blood 41 (1973) 877–891.
[43] T.W. Traut, Physiological concentrations of purines and pyrimidines, Mol Cell Biochem 140 (1994) 1–22.